

GENERAL INSTRUCTIONS

- Authors: Carefully check the page proofs (and coordinate with all authors); additional changes or updates WILL NOT be accepted after the article is published online/print in its final form. Please check author names and affiliations, funding, as well as the overall article for any errors prior to sending in your author proof corrections.
- Authors: Please check ALL author names for correct spelling, abbreviations, and order of first and last name in the byline, affiliation footnote, and bios.
- Authors: We cannot accept new source files as corrections for your article. If possible, please annotate the PDF proof we have sent you with your corrections and upload it via the Author Gateway. Alternatively, you may send us your corrections in list format. You may also upload revised graphics via the Author Gateway.
- Authors: Please note that once you upload your changes, they will be entered and your article finalized. The proofing process is now complete and your article will be sent for final publication and printing. If you would like an additional proof to review, this should be noted as it is not IEEE policy to send multiple proofs. Once your article is posted on Xplore, it is considered final and the article of record. No further changes will be allowed at this point so please ensure scrutiny of your final proof.
- Authors: Unless invited or otherwise informed, a mandatory Excessive Article Length charges will be incurred if your article is over the page limit set by the society in the Information for Authors.

QUERIES

- Q1. Author: Please provide the required affiliation (department, organization, city/state, postal code, country, and email address) for all the authors.
- Q2. Author: Please confirm or add details for any funding or financial support for the research of this article.
- Q3. Author: Please specify the corresponding author's name and email address along with the ORCID.
- Q4. Author: Please update Refs. [2], [3], [17], and [18], if already published.
- Q5. Author: Please check whether Ref. [6] is correct as set.

Letters

Narrowband and Wideband Dual-Mode Wireless Power Transfer System With a Single Transmitter

Enes Ayaz^{ID}, Oğün Altun^{ID}, Ozgur Gulsuna^{ID}, and Ozan Keysan^{ID}

Abstract—This study introduces a dual-mode wireless power transfer system for multistandard wireless charging products. The system allows two receivers to operate concurrently at narrowband and wideband frequencies using the proposed sinusoidal pulse width modulation (SPWM). Conventional SPWM does not provide independent control of switching and sideband harmonics, which are required for dual-mode excitation. We propose a new hybrid carrier and reference phase shift method to provide independent control of the reference, switching, and sideband harmonics. A prototype has been developed to validate power transfer at both narrowband (951 and 1190 kHz) and wideband (100 and 1190 kHz) frequency operations.

Index Terms—Dual-mode wireless power transfer, multistandard wireless charging, sinusoidal pulse width modulation (SPWM), wireless power transfer (WPT).

NOMENCLATURE

f_R	Reference (fundamental) frequency [Hz].
f_C	Carrier (switching) frequency [Hz].
f_L	Lower sideband ($f_R - 2f_o$) [Hz].
f_H	Higher sideband ($f_C - 2f_o$) [Hz].
$S_{A,B}$	Switching function of leg A or B.
J_k	k th order Bessel function.
m_a	Modulation index.
$\theta_{R(A,B)}$	Reference phases of leg A or B [$^\circ$].
$\theta_{CA,B}$	Carrier phases of leg A or B [$^\circ$].
$\Delta\theta_C$	The amount of carrier phase shift ($\theta_{CA} - \theta_{CB}$) [$^\circ$].
$\Delta\theta_R$	The amount of reference phase shift ($\theta_{RA} - \theta_{RB}$) [$^\circ$].
\hat{V}_{AB}	Inverter voltage [V_{peak}].
V_{dc}	Dc-link voltage [V].
V_{OUT}	Output voltage of WPT system [V].
V_{RX}	Output voltage of WPT system [V_{rms}].
ω	Operation frequency of WPT [rad/sec].
$L_{Rx1,2}$	Rx inductances of each channel [H].
L_{Tx}	Tx inductance [H].
$M_{1,2}$	Mutual inductances of each channel [H].
$C_{Rx1,2}$	Rx capacitances [F].

C_{Tx}	Tx capacitance [F].
$R_{L1,2}$	Load resistances of each channel [Ω].

I. INTRODUCTION

RECENT developments in wireless power transfer (WPT) technologies have encouraged wireless charging devices in robotics and consumer electronics [1]. Various WPT standards that regulate commercial devices have also given opportunities for WPT systems to spread in these applications. One of the most common standards is Qi by the wireless power consortium (WPC) [2]. In this standard, 110–205 kHz operating frequency range is adopted for low-power devices (5–15 W) [3]. In addition, 80–300 kHz operating frequency range is specified for medium-power (30–65 W) applications [4]. On the other hand, the Alliance for Wireless Power (A4WP) supports power transfer below 30 W in the operating frequency of 6.78 MHz with ± 15 kHz control range, and Power Matters Alliance (PMA) permits power below 5 W in the operating frequency range of 277–357 kHz [3], [5], [6]. Other frequency bands can also be utilized in various devices. For instance, 300–500 kHz range can be used in consumer devices for up to 5 W power.

The main advantages of WPT systems are increased safety and portability of the devices. In addition to these advantages, another benefit of wireless charging is its potential ability to charge multiple devices simultaneously using a single transmitter. For instance, it could wirelessly charge simultaneously several mobile phones and headphones from different manufacturers on a single pad. This capability has the potential to reduce costs and save space. However, at this point, it is significant to note that current standards for wireless charging are not universal and compatible. The lack of interoperability due to this incompatibility poses a challenge when desiring to utilize a single device with multiple products. Therefore, achieving interoperability among these standards would result in cost savings and making wireless charging widespread. For this aim, WPT systems with single-transmitter (single-Tx) and dual-receivers (dual-Rx) gain popularity [7], [8], [9], [10], [11], [12], [13], [14].

These systems utilize multiple coils and a dual-frequency inverter; thus, they can transmit power at two frequencies, which can be categorized as wideband and narrowband, according to their different operating frequencies. Wideband and narrowband

Q2 Received 24 June 2024; revised 10 August 2024 and 11 September 2024;
Q3 accepted 30 September 2024.

Color versions of one or more figures in this article are available at
<https://doi.org/10.1109/TPEL.2024.3474040>.

Digital Object Identifier 10.1109/TPEL.2024.3474040

systems differ significantly. Narrowband systems operate at closely spaced frequencies, presumably within the same standard. Wideband systems operate over a broader frequency range, encompassing signals from widely spaced frequencies and presumably different standards.

In [7], a dual-mode system is introduced to make the Tx device compatible with two WPT standards of A4WPT (6.78 MHz) and WPC/PMA (200 kHz). However, two set of coils and drivers are used in this system, increasing the complexity and cost. In [8], a single-inverter-based dual-frequency WPT system is proposed using the programmed PWM method, which provides both narrowband and wideband operations. However, this method is computationally complex and requires offline algorithms, which is not feasible for dynamic systems. In [12], time multiplication method is proposed to achieve power transfer at 100, 200, and 300 kHz by sequentially enabling the receivers. However, it requires negative gate voltages to avoid the reverse conduction of GaN switches. In [13], multifrequencies are achieved by comparing superimposed sinusoidal reference signals with high-frequency triangular carrier signals. However, in this method, the switching frequency is higher than the operating frequency of the WPT system, which increases the switching losses. In [14], multifrequency operation is achieved by a multilevel inverter (MLI) with a switching frequency lower than its two-level alternatives. However, this system uses a higher number of switching components, and it can be utilized in just narrowband operation. In this study, concurrent power transfer at dual-frequency (multistandards) is achieved by a single converter which is driven by a novel dual-frequency modulation technique. The proposed system can be applied to both narrowband and wideband operations. The main contribution of the study can be listed as follows.

- 1) A single converter is utilized to achieve a multistandard concurrent WPT system, reducing the system's cost.
- 2) The novel modulation method is easily implemented without extra computational burden.
- 3) The proposed system can be applied to both narrowband and wideband operations.
- 4) The proposed method guarantees that the switching frequency is near the operating frequencies, reducing the switching losses.

II. SYSTEM STRUCTURE AND PROPOSED METHOD

The proposed system is versatile and can work with various topologies. Fig. 1 shows a dual-mode WPT system configuration. In this system, a full-bridge (FB) converter generates dual-frequency output voltages that excite the single Tx coil.

Since the Tx side should let both frequencies to pass through, a dual-frequency compensation circuit is introduced, which will be explained later, while the Rx sides are compensated by only series capacitors. Therefore, Rx coils become selective and operate at different frequencies: f_1 and f_2 .

A. Dual Frequency Strategy Using SPWM

Conventionally, sinusoidal pulse width modulation (SPWM) is generated by comparing a high-frequency carrier (switching)

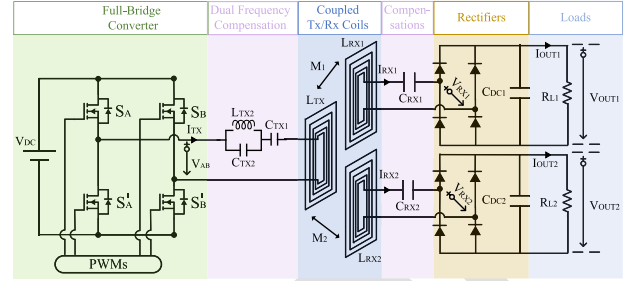


Fig. 1. Representative example of the proposed dual-mode WPT system.

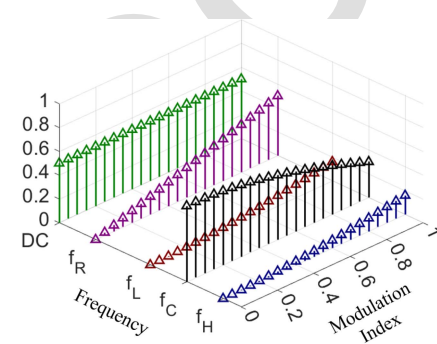


Fig. 2. Normalized magnitudes of the reference, carrier, and sideband harmonics with varying modulation index for the SPWM scheme (for a single leg).

signal and a reference (fundamental) signal. Its harmonic distribution can be calculated using double Fourier series analysis, as given in (1) where $\omega_R, \omega_C, \theta_R, \theta_C$, are angular frequencies and phases of reference and carrier signals, and J_o, J_k are the zeroth and k th order Bessel functions

$$\begin{aligned}
 S = & \frac{1}{2} + \frac{m_a}{2} \cos(\omega_R t + \theta_R) \\
 & + \frac{2}{\pi} \sum_{i=1}^{i=\infty} J_o\left(i \frac{\pi}{2} m_a\right) \sin\left(i \frac{\pi}{2}\right) \cos(i(\omega_C t + \theta_C)) \\
 & + \frac{2}{\pi} \sum_{i=1}^{i=\infty} \sum_{k=-\infty}^{k=\infty} \left[\frac{1}{i} J_k\left(i \frac{\pi}{2} m_a\right) \sin\left((i+k) \frac{\pi}{2}\right) \right] \left[\cos(i(\omega_C t + \theta_C) + k(\omega_R t + \theta_R)) \right].
 \end{aligned} \quad (1)$$

Although utilizing only reference signals is a common practice, in this article, it is proposed that switching and sideband harmonics can also be utilized to achieve dual-frequency WPT systems. The magnitudes of reference, carrier, and sideband harmonics for the SPWM scheme are shown in Fig. 2. Hence, in a conventional SPWM scheme, the magnitude of the fundamental signal can be adjusted by the modulation index (m_a), whereas the magnitudes of other components also change with m_a . However, dual-mode WPT systems require independent and concurrent control of two separate frequencies. Accordingly, additional control parameters should be introduced if the components of switching and its sideband harmonics are utilized.

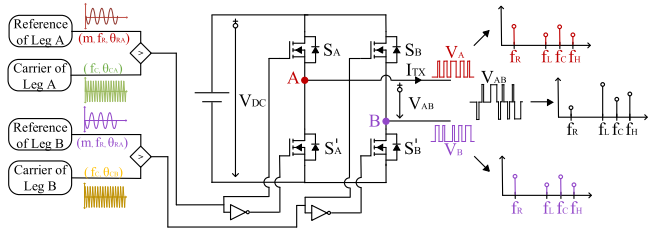


Fig. 3. Proposed modulation scheme of the hybrid control.

154 B. Proposed Control Method

155 In the proposed method, a hybrid carrier and a reference
156 phase shift control are applied to the SPWM method so that
157 independent dual-frequency at the output voltage of the FB
158 converter can be achieved. The proposed modulation scheme is
159 shown in Fig. 3 where separately controlled carrier and reference
160 signals generate the node A and the node B voltages.

161 The normalized output voltages (over dc-link voltage) for
162 each frequency component (reference (V_{ABf_R}), lower sideband
163 (V_{ABf_L}), carrier (V_{ABf_C}), and higher sideband (V_{ABf_H})) can
164 be calculated as in (2)–(5) by using the switching function in (1)
165 with taking ($i = 0, i = 1$), ($i = 1, k = -2$), and ($i = 1, k =$
166 2), and using different carrier and reference phases

$$V_{ABf_R}(t) = \frac{m_a}{2} \left[\cos(\omega_R t + \theta_{R_A}) - \cos(\omega_R t + \theta_{R_B}) \right] \quad (2)$$

$$V_{ABf_L}(t) = \frac{2}{\pi} J_2 \left(\frac{\pi}{2} m_a \right) \left[\cos(\omega_C t - 2\omega_R t + \theta_{C_B} - 2\theta_{R_B}) - \cos(\omega_C t - 2\omega_R t + \theta_{C_A} - 2\theta_{R_A}) \right] \quad (3)$$

$$V_{ABf_C}(t) = \frac{2}{\pi} J_o \left(\frac{\pi}{2} m_a \right) \left[\cos(\omega_C t + \theta_{C_A}) - \cos(\omega_C t + \theta_{C_B}) \right] \quad (4)$$

$$V_{ABf_H}(t) = \frac{2}{\pi} J_2 \left(\frac{\pi}{2} m_a \right) \left[\cos(\omega_C t + 2\omega_R t + \theta_{C_B} + 2\theta_{R_B}) - \cos(\omega_C t + 2\omega_R t + \theta_{C_A} + 2\theta_{R_A}) \right]. \quad (5)$$

167 It is observed that the magnitudes of these components can
168 be adjusted independently by controlling the phases of reference
169 and carrier signals. The control parameters and their affecting
170 components are shown in Table I.

171 Now, selecting any two frequencies respecting the operation
172 of narrowband or wideband is required as follows.

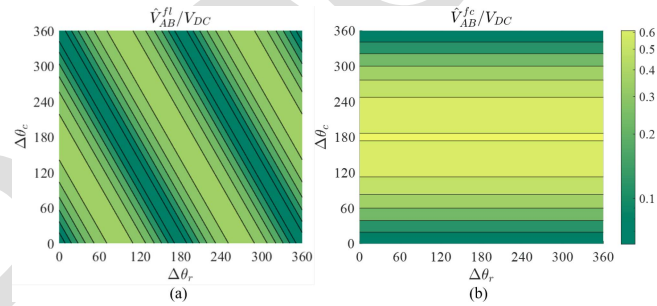
- 173 1) *Wideband operation:* The reference component can be
174 used as the lower frequency, and the carrier component
175 can be used as the higher frequency.
- 176 2) *Narrowband operation-I:* The lower sideband component
177 can be used for the lower frequency and the carrier com-
178 ponent can be used for the higher frequency.

TABLE I
CONTROL PARAMETERS AND OPERATIONS OF SPWM COMPONENTS

Control parameter	V_{ABf_R}	V_{ABf_L}	V_{ABf_C}	V_{ABf_H}
Modulation index (m_a)	±	±	±	±
Reference phase (θ_R)	±	±	0	±
Carrier phase (θ_C)	0	±	±	±
Operation	V_{ABf_R}	V_{ABf_L}	V_{ABf_C}	V_{ABf_H}
Wideband operation	Selected	–	Selected	–
Narrowband operation-I	–	Selected	Selected	–
Narrowband operation-II	–	–	Selected	Selected

±: can be changed by the control parameter.

0: cannot be changed by the control parameter.

Fig. 4. Narrowband operation. (a) Normalized voltage at f_L . (b) Normalized voltage at f_C .

- 179 3) *Narrowband operation-2:* The carrier component can be
180 used for the lower frequency and the higher sideband
181 component can be used for the higher frequency.

182 C. Narrowband Operation

183 Although there are two options in the narrowband operation,
184 in this section, the f_L and f_C are utilized to achieve dual-
185 frequency of f_1 and f_2 , and it is assumed that f_1 is the lower
186 one. The reference and carrier signals should be $f_R = \frac{f_2 - f_1}{2}$
187 and $f_C = f_2$, respectively. The peak value of the components
188 at f_L and f_C can be calculated in phasor domain by using (3)
189 and (4) as given in (6) and (7) where $\Delta\theta_C = \theta_{CA} - \theta_{CB}$, and
190 $\Delta\theta_R = \theta_{RA} - \theta_{RB}$

$$\hat{V}_{ABf_L} = V_{dc} \frac{2}{\pi} J_2 \left(\frac{\pi}{2} m_a \right) \sqrt{1 - \cos(\Delta\theta_C - 2\Delta\theta_R)} \quad (6)$$

$$\hat{V}_{ABf_C} = V_{dc} \frac{2}{\pi} J_o \left(\frac{\pi}{2} m_a \right) \sqrt{1 - \cos(\Delta\theta_C)}. \quad (7)$$

191 In this operation, it is proper to select m_a as 1 since the
192 achievable voltage ranges for both frequencies are compatible
193 at this point, as can be seen in Fig. 2(a).

194 For that m_a is 1, the normalized voltages (over V_{dc}) of \hat{V}_{ABf_C}
195 and \hat{V}_{ABf_L} are drawn in Fig. 4 for changing $\Delta\theta_c$ and $\Delta\theta_r$. It is
196 observed that while the normalized voltages at f_C (f_2) can be
197 adjusted in the range of [0, 0.601], the normalized voltages at f_L
198 (f_1) can be adjusted in the range of [0, 0.318]. The normalized
199 voltage ranges are swapped if we use f_H instead of f_L . One of
200 these two operations can be selected or switched online based
201 on the required power ratings of the Rx sides.

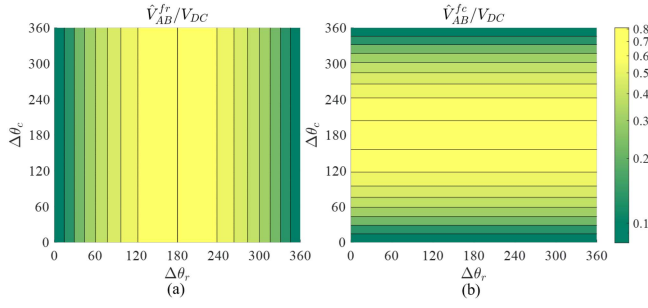


Fig. 5. Wideband operation. (a) Normalized voltage at f_R . (b) Normalized voltage at f_C .

202 D. Wideband Operation

203 In the wideband operation, the f_R component is used to
204 achieve the lower frequency (f_1), and f_C is used to obtain the
205 higher frequency component (f_2). The peak value of f_R and f_C
206 can be calculated in the phasor domain by using (2) and (4), and
207 they are given in (8) and (9)

$$\hat{V}_{AB}^{fr} = V_{dc} m_a \sqrt{\frac{1 - \cos(\Delta\theta_R)}{2}} \quad (8)$$

$$\hat{V}_{AB}^{fc} = V_{dc} \frac{2}{\pi} J_o \left(\frac{\pi}{2} m_a \right) \sqrt{1 - \cos(\Delta\theta_C)}. \quad (9)$$

208 In this operation, it is proper to select m_a as 0.8 since the
209 achievable voltage ranges for both frequencies are equal at
210 this point, as can be seen in Fig. 2(a). For that m_a is 0.8, the
211 normalized voltages (over V_{dc}) of \hat{V}_{AB}^{fr} and \hat{V}_{AB}^{fc} are drawn
212 in Fig. 5 for changing the control parameters of $\Delta\theta_C$ and $\Delta\theta_R$.
213 It is observed that both normalized voltages at f_R (f_1) and f_C
214 (f_2) can be adjusted in the range of [0, 0.81].

215 III. DISCUSSIONS AND FURTHER INVESTIGATIONS

216 A. Dual-Frequency Compensation System

217 A dual-frequency compensation system on the transmitter
218 side operates at both frequencies, while series capacitors set
219 the receiver sides to their respective resonant frequencies. This
220 article focuses specifically on dual-frequency excitation by using
221 the modulation method, so we present the values and the type of
222 compensation circuit employed rather than delving into the de-
223 sign of coil and compensation system, which can be found in the
224 literature [15], [16]. Fig. 1 shows the diagram of dual-frequency
225 compensation circuit, and Table II lists the circuit parameters of
226 both wideband and narrowband operations.

227 B. Gain Response and the Interference Between Receivers

228 The gain responses of receivers for narrowband and wideband
229 operations are shown in Fig. 6.

230 Notably, while almost no interaction occurs between the
231 receivers in a wideband operation, the narrowband operation
232 introduces mutual influence. This influence changes the effec-
233 tive gain for dual-frequency excitation, so the operating phase
234 shifts should be adjusted to account for this interference effect.
235 Moreover, optimization of the compensation method or proper

TABLE II
DUAL-RECEIVER WPT SYSTEM PARAMETERS

Parameters	Simulation value	Experimental value
Transmitter inductance	L_{TX}	$48\mu H$
Receiver inductances	L_{RX1}	$75\mu H$
Narrowband compensation inductance	L_{TX}	$1.5\mu H$
Wideband compensation inductance	L_{TX}	$28\mu H$
Narrowband transmitter compensation capacitances	C_{TX1}	$454pF$
Narrowband receiver compensation capacitances	C_{RX1}	$13.2nF$
Wideband transmitter compensation capacitances	C_{TX2}	$236pF$
Wideband receiver compensation capacitances	C_{RX2}	$340pF$
Narrowband load resistances	R_{L1}	68Ω
Wideband load resistances	R_{L2}	4.7Ω
Mutual inductance	M_1	$6\mu H$
	M_2	$6\mu H$

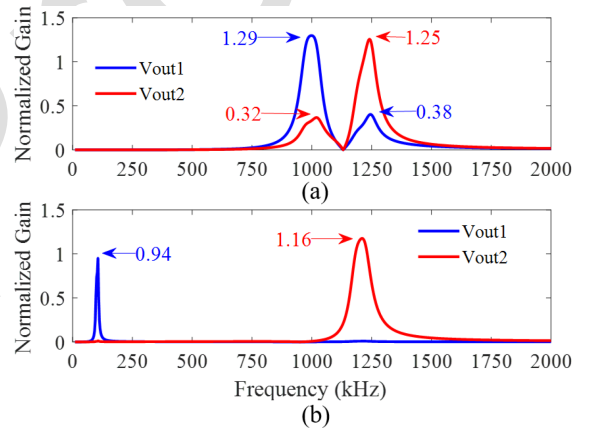


Fig. 6. Gain response of the dual receivers WPT system. (a) Narrowband operation. (b) Wideband operation.

TABLE III
DC-LINK UTILIZATION RATIO OF THE PROPOSED MODULATION TECHNIQUE

	Voltage gain at f_1	Voltage gain at f_2
Wideband operation	0.81	0.81
Narrowband operation	0.318	0.601

frequency selection can be recommended to mitigate this effect. For example, anti-interference compensation on the receiver sides might be suitable [17]. In addition, the cross-coupling between receivers should be minimized, since it increases the interference ratio.

241 C. DC-Link Utilization Ratio of the Proposed Modulation 242 Method

The proposed modulation allows for voltage control at two frequencies, which are limited to specific dc-link utilization ratios, which are given in Table III. The utilization ratios of the dual frequency excitation vary based on frequency selection in the other modulation techniques. In a system using superposition in SPWM, the summation of two signals should be at a maximum of 1 [13]. If you use antiphase signals, you can increase the utilization ratio. In this article using SHEPWM, it is observed

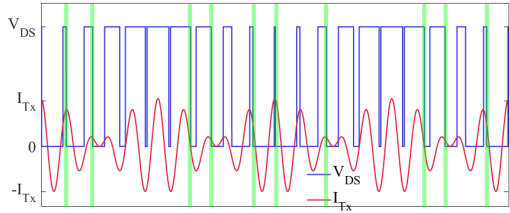


Fig. 7. Exemplary waveforms of drain-source voltage (V_{DS}) and transmitter current (I_{Tx}) with marked ZVS points in green. 10 of 20 turn-ON instances achieve ZVS.

that the utilization ratio typically range between 0.3 and 0.9 [8]. Moreover, when two distinct frequencies are excited with two half-bridges, a utilization ratio of $0.5 \times 4/\pi = 0.64$ can be achieved for both frequencies. Our recommended wideband modulation exceeds the gains of a two-half-bridge configuration. In the narrowband, one frequency could be excited with approximately these values while the other frequency component has a lower gain.

D. Dual-Receiver Output Regulation

The first control method in the proposed system is to adjust the carrier and reference phase shifts since you can change the voltage gain of the modulation. The second method is to detune the operating frequency since the proposed modulation technique can easily accommodate various frequencies. Furthermore, the active rectifiers at the receiver sides might be utilized to regulate the output voltages finely. In this article, the control loop is not closed, and the output voltages have been controlled by introducing phase shifts.

E. Zero Voltage Switching (ZVS) Conditions

Conventional WPT systems act as an inductive load, causing the current to lag when operating above the resonant frequency (unless in bifurcation condition). Before setting the gate signal high, a dead-time (blanking time) is given between each leg's top and bottom switches to prevent short-circuiting of the dc-link capacitors. During this dead-time period, the load current discharges the output capacitances of the switches. The inductive operation and lagged current ensure that the current direction always aligns with the discharging of the capacitors. As a result, the switches achieve ZVS at turn-ON. However, in the proposed system, the existence of multifrequency components in the transmitter current disrupts this assurance, even if the system operates in the inductive region at each frequency. Nevertheless, the proposed system may still have partial ZVS points, depending on the magnitudes and frequencies of the components of the Tx currents. An example operating point is depicted in Fig. 7, with the ZVS points marked.

Therefore, the system needs to be designed assuming hard-switching conditions. This design remains in the worst-case scenario. However, the efficiency might be higher in practical use than calculated, thanks to the partial ZVS.

F. Efficiency Analysis

The system's power losses are primarily due to the losses of inverter (P_{inv}), rectifier (P_{rec}), and network (P_{net}), as given in [18]. Then, overall system efficiency can be calculated by

$$\eta = \frac{P_{out}}{P_{in}} = \frac{P_{out}}{P_{out} + P_{inv} + P_{rec} + P_{net}} \quad (10)$$

where P_{in} is input power, and P_{out} is output power. First, the inverter loss can be split into two parts as given in

$$P_{inv} = P_c + P_{sw} \quad (11)$$

where P_c is the conduction loss, and P_{sw} is the switching loss. In conventional 1Tx–1Rx WPT systems, achieving ZVS, which reduces switching losses significantly, is ensured by operating in the inductive region near the zero-phase angle (ZPA). Then, the inverter loss, when in ZVS operation, can be considered conduction loss. However, in the proposed 1Tx–2Rx system, the ZVS might not be ensured, and the inverter loss should be calculated in hard-switching operation, as given by

$$P_{inv} = P_c = I_{Tx}^2 r_{ds} + f_{sw}(E_{sw-ZCS} + E_{sw-OL}) \quad (12)$$

where I_{Tx} is the rms value of the Tx current, r_{ds} is the MOSFET ON-state resistance, f_{sw} is the switching frequency, E_{sw-ZCS} is the zero current switching energy due to output capacitances of the switches, and E_{sw-OL} is the overlapping switching energy because of switching speed of switches as dv/dt and di/dt . Moreover, operating near ZPA can also decrease conduction losses by lowering the rms of the Tx current since the power factor becomes unity. Second, the rectifier operates in continuous conduction mode, resulting in pure sinusoidal current. Therefore, the loss can be calculated by

$$P_{rec} = \left(\frac{2\sqrt{2}}{\pi} V_F I_{Rx1} + r_F I_{Rx1}^2 \right) + \left(\frac{2\sqrt{2}}{\pi} V_F I_{Rx2} + r_F I_{Rx2}^2 \right) \quad (13)$$

where V_F and r_F are the opening voltage and ON-state resistance of the diodes, and I_{Rx1} and I_{Rx2} are receiver currents. Finally, the loss from network elements, such as passive elements, such as coils and capacitors, depends on the rms value and frequency of the currents of the Tx and Rx sides. The loss can be calculated by

$$P_{net} = I_{Tx}^2 r_{net_{Tx}} + I_{Rx1}^2 r_{net_{Rx1}} + I_{Rx2}^2 r_{net_{Rx2}} \quad (14)$$

where $r_{net_{Tx}}$, $r_{net_{Rx1}}$, and $r_{net_{Rx2}}$ are the representative resistances for network losses for the Tx and Rx sides.

The analysis conducted previously shows that the proposed system might have higher inverter loss than conventional 1Tx–1Rx systems due to the absence of ZVS. The other losses are almost equal to those of conventional systems if we make a fair comparison. Yet, the incorporation of wideband gap semiconductors plays a crucial role. It allows for an increase in the dv/dt , thereby reducing switching losses and enabling hard-switching opportunities at higher switching frequencies. Consequently, the overall system may have a switching loss that forms a minority portion of the total loss. In such a scenario, reducing costs

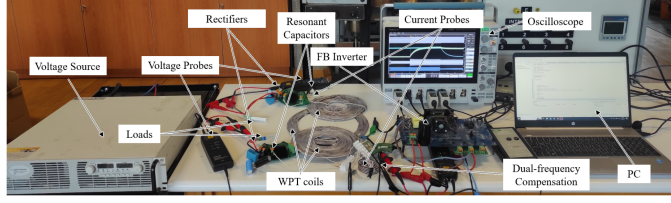


Fig. 8. Experimental setup of dual-mode WPT System.

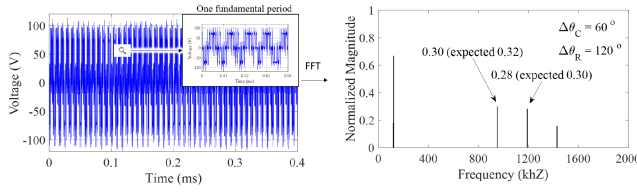


Fig. 9. Inverter output voltage and its harmonics spectrum for narrowband operation. The fundamental frequency is 119.5 kHz, and the switching frequency is 1190 kHz. The modulation index is 1.

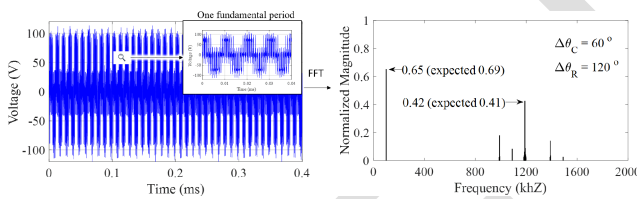


Fig. 10. Inverter output voltage and its harmonics spectrum for wideband operation. The fundamental frequency is 100 kHz, and the switching frequency is 1190 kHz. The modulation index is 0.8.

333 achieved by decreasing the number of inverters can offset the
334 efficiency decrease due to switching loss.

335 IV. EXPERIMENTAL VALIDATION

336 An experimental setup, shown in Fig. 8, is established to
337 validate the proposed system. The system parameters are shown
338 in Table II. In the setup, we wound the coils using 1 mm
339 diameter litz wires. The oscilloscope was a six-channel Tek-
340 tronix MSO46. We employed PEM CWTMini HF03B current
341 probes for ac current measurement and Tektronix THDP0100
342 differential probes for voltage measurement. The power sup-
343 ply was an Agilent N8739A. To generate the proposed mod-
344 ulation, the TI C2000 TMS320F28379D microcontroller is
345 utilized.

346 A. Dual-Mode Inverter Tests

347 The voltage waveforms of V_{AB} for both narrowband and
348 wideband operations are shown in Figs. 9 and 10. As expected, it
349 is observed that the voltages of each frequency can be indepen-
350 dently controlled by $\Delta\theta_R$ and $\Delta\theta_C$. There are slight differences
351 between experimental results and mathematical calculations,
352 which are at a maximum of 6%.

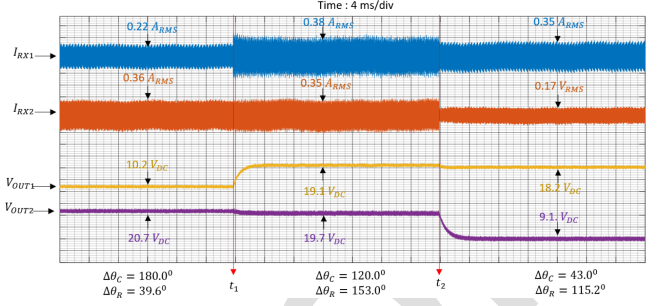
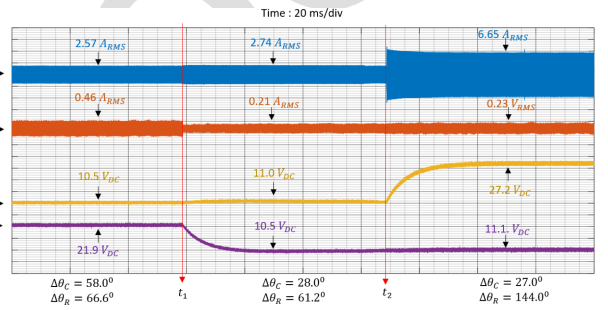
Fig. 11. Narrowband operation of dual-mode WPT system. m_a is 1, f_L is 951 kHz, and f_C is 1190 kHz.Fig. 12. Wideband operation of dual-mode WPT system. m_a is 0.8, f_L is 100 kHz, and f_C is 1190 kHz.

TABLE IV
POWER TRANSFER EFFICIENCIES FOR DIFFERENT OPERATING POINTS

	Carrier phase shift	Reference phase shift	Power transfer efficiency
Narrowband operation	180°	39.6°	74.6 %
	120°	153°	76.3 %
	43°	115.2°	76.0 %
Wideband operation	58°	66.2°	75.3%
	28°	61.2°	75.7 %
	27°	144.0°	75.5 %

B. Dual-Mode WPT System Tests

The Rxs and outputs' currents and V_{AB} voltage are obtained for narrowband and wideband operations, as given in Figs. 11 and 12. Transient analysis was performed to study the impact of different operating phase shifts in both wideband and narrowband operations. It's important to note that the voltages in this experimental setup may deviate slightly from the analytical calculations due to dead time and other nonlinearities since closed-loop control was not utilized. Furthermore, in narrowband operation, the interference between receivers necessitates minor updates to the phase shifts in addition to the analytical calculations in order to compensate for the effect.

C. Dual-Mode WPT System Power Transfer Efficiencies

The efficiency measurements for both narrowband and wideband operations in various conditions are provided in Table IV. In all cases, it was observed that the efficiencies were about 75%. Our proposed system has a key advantage that could potentially lead to increased efficiency by reducing the required switching

TABLE V
COMPARISON WITH EXISTING STUDIES IN THE LITERATURE

	Channel mode	Tx device	Offline algorithm	Operating frequency
[7]	2 (WB)	Two-2LC	NR	$= f_s$
[8]	2 (NB/WB)	Single-2LC	R	$\leq f_s$
[13]	2 (NB)	Single-2LC	NR	$< f_s$
[14]	2 (NB)	Single-MLI	NR	$\geq f_s$
This work	2 (NB/WB)	Single-2LC	NR	$= f_s$

2LC : Two level converter, MLI : Multi level inverter,

NB : Narrowband, WB :Wideband, R : Required, NR :Not required.

371 frequencies. Still, it is also worth considering optimizing the coil
372 and compensation systems to improve efficiency further.

373 V. COMPARISON WITH LITERATURE

374 Existing studies are compared with the proposed system in
375 Table V. Unlike the approaches presented in [7] and [14], our
376 proposed system does not require extra switches, which reduces
377 the cost and complexity. In contrast to the system discussed
378 in [13], our system allows both wideband and narrowband
379 operations and has operating frequencies near the switching
380 frequency, decreasing switching losses. Unlike the method out-
381 lined in [8], our system does not require an offline algorithm
382 to calculate the different quiescent points, thereby enabling
383 dynamic operations.

384 VI. CONCLUSION

385 In this letter, concurrent power transfer at dual frequency was
386 achieved by a single converter using a novel hybrid reference and
387 carrier phase shifts method of SPWM, allowing for a control-
388 lable dual-frequency output. This versatile modulation method
389 is applicable to narrowband and wideband operations, and it
390 enables the use of single Tx device by multiple standards. The
391 experimental setup was established to confirm the effectiveness
392 of the proposed modulation technique, and a good agreement
393 was observed between experimental results and mathematical
394 calculations. Further, the proposed system offers several advan-
395 tages, such as reduced switching components and lower switch-
396 ing frequency, resulting in increased efficiency and decreased
397 system cost. Consequently, the proposed system enhances the
398 adoption of dual-band WPT systems that support multistandard
399 usage in robotics and consumer electronics.

400 REFERENCES

- 401 [1] W. Jin, A. T. L. Lee, S.-C. Tan, and S. Y. R. Hui, "Single-inductor multiple-
402 output inverter with precise and independent output voltage regulation,"
403 *IEEE Trans. Power Electron.*, vol. 35, no. 10, pp. 11222–11234, Oct. 2020.

- 404 [2] "The QI wireless power transfer system power class 0 specification,"
405 Apr. 2016. [Online]. Available: <https://www.wirelesspowerconsortium.com/>
- 406 [3] "Nxp wireless power solutions," NXP, May 2017. Accessed: Mar.
407 20, 2023. [Online]. Available: <https://www.nxp.com/docs/en/supporting-information/BL-Micro-NXP-Wireless-Charging-Solutions-Beta-Chen.pdf>
- 408 [4] Y. Xiao, C. Liu, Y. Huang, and S. Liu, "Concurrent wireless power
409 transfer to multiple receivers with additional resonant frequencies and
410 reduced power switches," *IEEE Trans. Ind. Electron.*, vol. 67, no. 11,
411 pp. 9292–9301, Nov. 2020.
- 412 [5] J. Wu, L. Bie, W. Kong, P. Gao, and Y. Wang, "Multi-frequency multi-
413 amplitude superposition modulation method with phase shift optimization
414 for single inverter of wireless power transfer system," *IEEE Trans. Circuits
415 Syst. I: Reg. Papers*, vol. 68, no. 5, pp. 2271–2279, May 2021.
- 416 [6] *A Wireless Power Transfer System Baseline System Specification (BSS)*,
417 Standard A4WP-S-0001 v1.3, Jan. 2014.
- 418 [7] D. Ahn and P. P. Mercier, "Wireless power transfer with concurrent 200-
419 kHz and 6.78-MHz operation in a single-transmitter device," *IEEE Trans.
420 Power Electron.*, vol. 31, no. 7, pp. 5018–5029, Jul. 2016.
- 421 [8] C. Zhao and D. Costinett, "GaN-based dual-mode wireless power transfer
422 using multifrequency programmed pulse width modulation," *IEEE Trans.
423 Ind. Electron.*, vol. 64, no. 11, pp. 9165–9176, Nov. 2017.
- 424 [9] F. Liu, Y. Yang, Z. Ding, X. Chen, and R. M. Kennel, "A multifrequency
425 superposition methodology to achieve high efficiency and targeted power
426 distribution for a multiload MCR WPT System," *IEEE Trans. Power
427 Electron.*, vol. 33, no. 10, pp. 9005–9016, Oct. 2018.
- 428 [10] Z. Liu, M. Su, Q. Zhu, Y. Chao, S. Zang, and A. P. Hu, "A dual-frequency
429 three-dimensional 3-D WPT system with directional power transfer capa-
430 bility at two separately regulated outputs," *IEEE Trans. Emerg. Sel. Topics
431 Power Electron.*, vol. 11, no. 3, pp. 2514–2524, Jun. 2023.
- 432 [11] C. Qi, S. Huang, X. Chen, and P. Wang, "Individual output voltage
433 regulation method of multifrequency multireceiver simultaneous WPT
434 systems with a single inverter," *IEEE Trans. Emerg. Sel. Topics Power
435 Electron.*, vol. 11, no. 1, pp. 1245–1261, Feb. 2023.
- 436 [12] W. Jin, A. T. L. Lee, S.-C. Tan, and S. Y. Hui, "A gallium nitride
437 (GaN)-based single-inductor multiple-output (SIMO) inverter with multi-
438 frequency AC outputs," *IEEE Trans. Power Electron.*, vol. 34, no. 11,
439 pp. 10856–10873, Nov. 2019.
- 440 [13] C. Xia, N. Wei, H. Zhang, S. Zhao, Z. Li, and Z. Liao, "Multifre-
441 quency and multiload MCR-WPT system using hybrid modulation waves
442 SPWM control method," *IEEE Trans. Power Electron.*, vol. 36, no. 11,
443 pp. 12400–12412, Nov. 2021.
- 444 [14] Y. Liu, C. Liu, X. Gao, and S. Liu, "Design and control of a decoupled mul-
445 tichannel wireless power transfer system based on multilevel inverters,"
446 *IEEE Trans. Power Electron.*, vol. 37, no. 8, pp. 10045–10060, Aug. 2022.
- 447 [15] Z. Zhang, X. Li, H. Pang, H. Komurcugil, Z. Liang, and R. Kennel,
448 "Multiple-frequency resonating compensation for multichannel transmis-
449 sion of wireless power transfer," *IEEE Trans. Power Electron.*, vol. 36,
450 no. 5, pp. 5169–5180, May 2021.
- 451 [16] C. Qi, H. Miao, Z. Lang, and X. Chen, "A generalized methodology to gen-
452 erate, amplify and compensate multi-frequency power for a single-inverter-
453 based MF-MR-S-WPT system," *IEEE Access*, vol. 8, pp. 181513–181525,
454 2020.
- 455 [17] X. Tian, J. Zhang, H. Wang, and S. M. Goetz, "Design and analysis of
456 automatic modulation and demodulation strategy in wireless power and
457 drive transfer system," *IEEE Trans. Ind. Electron.*, to be published, 2024,
458 doi: [10.1109/TIE.2024.3406885](https://doi.org/10.1109/TIE.2024.3406885).
- 459 [18] H. Liu, L. He, and B. Cheng, "Powerless fractional-order tun-
460 ing wireless power transfer system with zero phase angle input,"
461 *IEEE Trans. Circuits Syst. I: Reg. Papers*, to be published, 2024,
462 doi: [10.1109/TCSI.2024.3404647](https://doi.org/10.1109/TCSI.2024.3404647).

GENERAL INSTRUCTIONS

- Authors: Carefully check the page proofs (and coordinate with all authors); additional changes or updates WILL NOT be accepted after the article is published online/print in its final form. Please check author names and affiliations, funding, as well as the overall article for any errors prior to sending in your author proof corrections.
- Authors: Please check ALL author names for correct spelling, abbreviations, and order of first and last name in the byline, affiliation footnote, and bios.
- Authors: We cannot accept new source files as corrections for your article. If possible, please annotate the PDF proof we have sent you with your corrections and upload it via the Author Gateway. Alternatively, you may send us your corrections in list format. You may also upload revised graphics via the Author Gateway.
- Authors: Please note that once you upload your changes, they will be entered and your article finalized. The proofing process is now complete and your article will be sent for final publication and printing. If you would like an additional proof to review, this should be noted as it is not IEEE policy to send multiple proofs. Once your article is posted on Xplore, it is considered final and the article of record. No further changes will be allowed at this point so please ensure scrutiny of your final proof.
- Authors: Unless invited or otherwise informed, a mandatory Excessive Article Length charges will be incurred if your article is over the page limit set by the society in the Information for Authors.

QUERIES

- Q1. Author: Please provide the required affiliation (department, organization, city/state, postal code, country, and email address) for all the authors.
- Q2. Author: Please confirm or add details for any funding or financial support for the research of this article.
- Q3. Author: Please specify the corresponding author's name and email address along with the ORCID.
- Q4. Author: Please update Refs. [2], [3], [17], and [18], if already published.
- Q5. Author: Please check whether Ref. [6] is correct as set.

Letters

Narrowband and Wideband Dual-Mode Wireless Power Transfer System With a Single Transmitter

Enes Ayaz^{ID}, Oğün Altun^{ID}, Ozgur Gulsuna^{ID}, and Ozan Keysan^{ID}

Abstract—This study introduces a dual-mode wireless power transfer system for multistandard wireless charging products. The system allows two receivers to operate concurrently at narrowband and wideband frequencies using the proposed sinusoidal pulse width modulation (SPWM). Conventional SPWM does not provide independent control of switching and sideband harmonics, which are required for dual-mode excitation. We propose a new hybrid carrier and reference phase shift method to provide independent control of the reference, switching, and sideband harmonics. A prototype has been developed to validate power transfer at both narrowband (951 and 1190 kHz) and wideband (100 and 1190 kHz) frequency operations.

Index Terms—Dual-mode wireless power transfer, multistandard wireless charging, sinusoidal pulse width modulation (SPWM), wireless power transfer (WPT).

NOMENCLATURE

f_R	Reference (fundamental) frequency [Hz].
f_C	Carrier (switching) frequency [Hz].
f_L	Lower sideband ($f_R - 2f_o$) [Hz].
f_H	Higher sideband ($f_C - 2f_o$) [Hz].
$S_{A,B}$	Switching function of leg A or B.
J_k	k th order Bessel function.
m_a	Modulation index.
$\theta_{R(A,B)}$	Reference phases of leg A or B [$^\circ$].
$\theta_{CA,B}$	Carrier phases of leg A or B [$^\circ$].
$\Delta\theta_C$	The amount of carrier phase shift ($\theta_{CA} - \theta_{CB}$) [$^\circ$].
$\Delta\theta_R$	The amount of reference phase shift ($\theta_{RA} - \theta_{RB}$) [$^\circ$].
\dot{V}_{AB}	Inverter voltage [V_{peak}].
V_{dc}	Dc-link voltage [V].
V_{OUT}	Output voltage of WPT system [V].
V_{RX}	Output voltage of WPT system [V_{rms}].
ω	Operation frequency of WPT [rad/sec].
$L_{Rx1,2}$	Rx inductances of each channel [H].
L_{Tx}	Tx inductance [H].
$M_{1,2}$	Mutual inductances of each channel [H].
$C_{Rx1,2}$	Rx capacitances [F].

C_{Tx}	Tx capacitance [F].
$R_{L_{1,2}}$	Load resistances of each channel [Ω].

I. INTRODUCTION

RECENT developments in wireless power transfer (WPT) technologies have encouraged wireless charging devices in robotics and consumer electronics [1]. Various WPT standards that regulate commercial devices have also given opportunities for WPT systems to spread in these applications. One of the most common standards is Qi by the wireless power consortium (WPC) [2]. In this standard, 110–205 kHz operating frequency range is adopted for low-power devices (5–15 W) [3]. In addition, 80–300 kHz operating frequency range is specified for medium-power (30–65 W) applications [4]. On the other hand, the Alliance for Wireless Power (A4WP) supports power transfer below 30 W in the operating frequency of 6.78 MHz with ± 15 kHz control range, and Power Matters Alliance (PMA) permits power below 5 W in the operating frequency range of 277–357 kHz [3], [5], [6]. Other frequency bands can also be utilized in various devices. For instance, 300–500 kHz range can be used in consumer devices for up to 5 W power.

The main advantages of WPT systems are increased safety and portability of the devices. In addition to these advantages, another benefit of wireless charging is its potential ability to charge multiple devices simultaneously using a single transmitter. For instance, it could wirelessly charge simultaneously several mobile phones and headphones from different manufacturers on a single pad. This capability has the potential to reduce costs and save space. However, at this point, it is significant to note that current standards for wireless charging are not universal and compatible. The lack of interoperability due to this incompatibility poses a challenge when desiring to utilize a single device with multiple products. Therefore, achieving interoperability among these standards would result in cost savings and making wireless charging widespread. For this aim, WPT systems with single-transmitter (single-Tx) and dual-receivers (dual-Rx) gain popularity [7], [8], [9], [10], [11], [12], [13], [14].

These systems utilize multiple coils and a dual-frequency inverter; thus, they can transmit power at two frequencies, which can be categorized as wideband and narrowband, according to their different operating frequencies. Wideband and narrowband

Q2 Received 24 June 2024; revised 10 August 2024 and 11 September 2024;
Q3 accepted 30 September 2024.

Color versions of one or more figures in this article are available at
<https://doi.org/10.1109/TPEL.2024.3474040>.

Digital Object Identifier 10.1109/TPEL.2024.3474040

systems differ significantly. Narrowband systems operate at closely spaced frequencies, presumably within the same standard. Wideband systems operate over a broader frequency range, encompassing signals from widely spaced frequencies and presumably different standards.

In [7], a dual-mode system is introduced to make the Tx device compatible with two WPT standards of A4WPT (6.78 MHz) and WPC/PMA (200 kHz). However, two set of coils and drivers are used in this system, increasing the complexity and cost. In [8], a single-inverter-based dual-frequency WPT system is proposed using the programmed PWM method, which provides both narrowband and wideband operations. However, this method is computationally complex and requires offline algorithms, which is not feasible for dynamic systems. In [12], time multiplication method is proposed to achieve power transfer at 100, 200, and 300 kHz by sequentially enabling the receivers. However, it requires negative gate voltages to avoid the reverse conduction of GaN switches. In [13], multifrequencies are achieved by comparing superimposed sinusoidal reference signals with high-frequency triangular carrier signals. However, in this method, the switching frequency is higher than the operating frequency of the WPT system, which increases the switching losses. In [14], multifrequency operation is achieved by a multilevel inverter (MLI) with a switching frequency lower than its two-level alternatives. However, this system uses a higher number of switching components, and it can be utilized in just narrowband operation. In this study, concurrent power transfer at dual-frequency (multistandards) is achieved by a single converter which is driven by a novel dual-frequency modulation technique. The proposed system can be applied to both narrowband and wideband operations. The main contribution of the study can be listed as follows.

- 1) A single converter is utilized to achieve a multistandard concurrent WPT system, reducing the system's cost.
- 2) The novel modulation method is easily implemented without extra computational burden.
- 3) The proposed system can be applied to both narrowband and wideband operations.
- 4) The proposed method guarantees that the switching frequency is near the operating frequencies, reducing the switching losses.

II. SYSTEM STRUCTURE AND PROPOSED METHOD

The proposed system is versatile and can work with various topologies. Fig. 1 shows a dual-mode WPT system configuration. In this system, a full-bridge (FB) converter generates dual-frequency output voltages that excite the single Tx coil.

Since the Tx side should let both frequencies to pass through, a dual-frequency compensation circuit is introduced, which will be explained later, while the Rx sides are compensated by only series capacitors. Therefore, Rx coils become selective and operate at different frequencies: f_1 and f_2 .

A. Dual Frequency Strategy Using SPWM

Conventionally, sinusoidal pulse width modulation (SPWM) is generated by comparing a high-frequency carrier (switching)

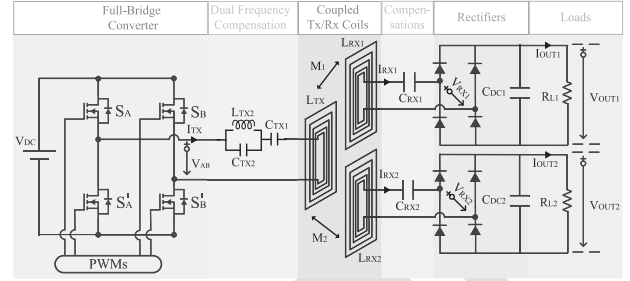


Fig. 1. Representative example of the proposed dual-mode WPT system.

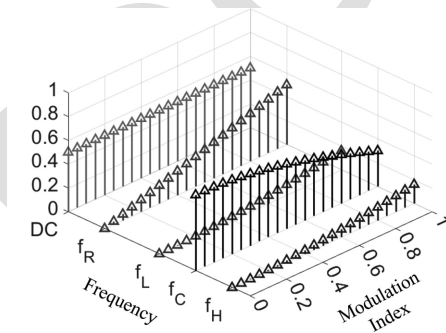


Fig. 2. Normalized magnitudes of the reference, carrier, and sideband harmonics with varying modulation index for the SPWM scheme (for a single leg).

signal and a reference (fundamental) signal. Its harmonic distribution can be calculated using double Fourier series analysis, as given in (1) where $\omega_R, \omega_C, \theta_R, \theta_C$, are angular frequencies and phases of reference and carrier signals, and J_o, J_k are the zeroth and k th order Bessel functions

$$\begin{aligned}
 S = & \frac{1}{2} + \frac{m_a}{2} \cos(\omega_R t + \theta_R) \\
 & + \frac{2}{\pi} \sum_{i=1}^{i=\infty} J_o \left(i \frac{\pi}{2} m_a \right) \sin \left(i \frac{\pi}{2} \right) \cos(i(\omega_C t + \theta_C)) \\
 & + \frac{2}{\pi} \sum_{i=1}^{i=\infty} \sum_{k=-\infty}^{k=\infty} \left[\begin{array}{l} \frac{1}{i} J_k \left(i \frac{\pi}{2} m_a \right) \sin \left((i+k) \frac{\pi}{2} \right) \\ \cos(i(\omega_C t + \theta_C) + k(\omega_R t + \theta_R)) \end{array} \right]. \tag{1}
 \end{aligned}$$

Although utilizing only reference signals is a common practice, in this article, it is proposed that switching and sideband harmonics can also be utilized to achieve dual-frequency WPT systems. The magnitudes of reference, carrier, and sideband harmonics for the SPWM scheme are shown in Fig. 2. Hence, in a conventional SPWM scheme, the magnitude of the fundamental signal can be adjusted by the modulation index (m_a), whereas the magnitudes of other components also change with m_a . However, dual-mode WPT systems require independent and concurrent control of two separate frequencies. Accordingly, additional control parameters should be introduced if the components of switching and its sideband harmonics are utilized.

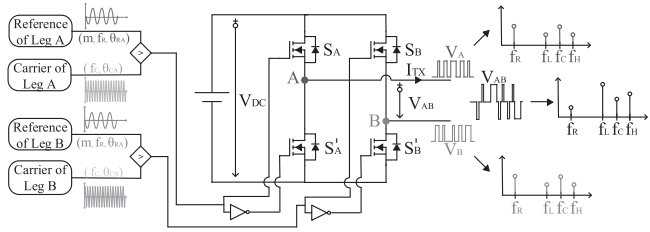


Fig. 3. Proposed modulation scheme of the hybrid control.

154 B. Proposed Control Method

155 In the proposed method, a hybrid carrier and a reference
156 phase shift control are applied to the SPWM method so that
157 independent dual-frequency at the output voltage of the FB
158 converter can be achieved. The proposed modulation scheme is
159 shown in Fig. 3 where separately controlled carrier and reference
160 signals generate the node A and the node B voltages.

161 The normalized output voltages (over dc-link voltage) for
162 each frequency component (reference ($V_{AB}^{f_R}$), lower sideband
163 ($V_{AB}^{f_L}$), carrier ($V_{AB}^{f_C}$), and higher sideband ($V_{AB}^{f_H}$)) can
164 be calculated as in (2)–(5) by using the switching function in (1)
165 with taking ($i = 0, i = 1$), ($i = 1, k = -2$), and ($i = 1, k =$
166 2), and using different carrier and reference phases

$$V_{AB}^{f_R}(t) = \frac{m_a}{2} \left[\cos(\omega_R t + \theta_{R_A}) - \cos(\omega_R t + \theta_{R_B}) \right] \quad (2)$$

$$V_{AB}^{f_L}(t) = \frac{2}{\pi} J_2 \left(\frac{\pi}{2} m_a \right) \left[\cos(\omega_C t - 2\omega_R t + \theta_{C_B} - 2\theta_{R_B}) - \cos(\omega_C t - 2\omega_R t + \theta_{C_A} - 2\theta_{R_A}) \right] \quad (3)$$

$$V_{AB}^{f_C}(t) = \frac{2}{\pi} J_o \left(\frac{\pi}{2} m_a \right) \left[\cos(\omega_C t + \theta_{C_A}) - \cos(\omega_C t + \theta_{C_B}) \right] \quad (4)$$

$$V_{AB}^{f_H}(t) = \frac{2}{\pi} J_2 \left(\frac{\pi}{2} m_a \right) \left[\cos(\omega_C t + 2\omega_R t + \theta_{C_B} + 2\theta_{R_B}) - \cos(\omega_C t + 2\omega_R t + \theta_{C_A} + 2\theta_{R_A}) \right]. \quad (5)$$

167 It is observed that the magnitudes of these components can
168 be adjusted independently by controlling the phases of reference
169 and carrier signals. The control parameters and their affecting
170 components are shown in Table I.

171 Now, selecting any two frequencies respecting the operation
172 of narrowband or wideband is required as follows.

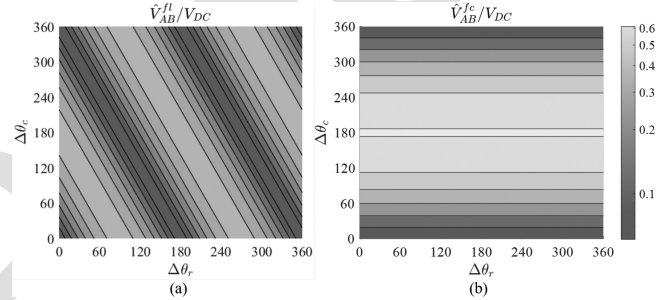
- 173 1) *Wideband operation:* The reference component can be
174 used as the lower frequency, and the carrier component
175 can be used as the higher frequency.
- 176 2) *Narrowband operation-I:* The lower sideband component
177 can be used for the lower frequency and the carrier com-
178 ponent can be used for the higher frequency.

TABLE I
CONTROL PARAMETERS AND OPERATIONS OF SPWM COMPONENTS

Control parameter	$V_{AB}^{f_R}$	$V_{AB}^{f_L}$	$V_{AB}^{f_C}$	$V_{AB}^{f_H}$
Modulation index (m_a)	±	±	±	±
Reference phase (θ_R)	±	±	0	±
Carrier phase (θ_C)	0	±	±	±
Operation	$V_{AB}^{f_R}$	$V_{AB}^{f_L}$	$V_{AB}^{f_C}$	$V_{AB}^{f_H}$
Wideband operation	Selected	—	Selected	—
Narrowband operation-I	—	Selected	Selected	—
Narrowband operation-II	—	—	Selected	Selected

±: can be changed by the control parameter.

0: cannot be changed by the control parameter.

Fig. 4. Narrowband operation. (a) Normalized voltage at f_L . (b) Normalized voltage at f_C .

- 179 3) *Narrowband operation-2:* The carrier component can be
180 used for the lower frequency and the higher sideband
181 component can be used for the higher frequency.

182 C. Narrowband Operation

183 Although there are two options in the narrowband operation,
184 in this section, the f_L and f_C are utilized to achieve dual-
185 frequency of f_1 and f_2 , and it is assumed that f_1 is the lower
186 one. The reference and carrier signals should be $f_R = \frac{f_2 - f_1}{2}$
187 and $f_C = f_2$, respectively. The peak value of the components
188 at f_L and f_C can be calculated in phasor domain by using (3)
189 and (4) as given in (6) and (7) where $\Delta\theta_C = \theta_{CA} - \theta_{CB}$, and
190 $\Delta\theta_R = \theta_{RA} - \theta_{RB}$

$$\hat{V}_{AB}^{f_L} = V_{dc} \frac{2}{\pi} J_2 \left(\frac{\pi}{2} m_a \right) \sqrt{1 - \cos(\Delta\theta_C - 2\Delta\theta_R)} \quad (6)$$

$$\hat{V}_{AB}^{f_C} = V_{dc} \frac{2}{\pi} J_o \left(\frac{\pi}{2} m_a \right) \sqrt{1 - \cos(\Delta\theta_C)}. \quad (7)$$

191 In this operation, it is proper to select m_a as 1 since the
192 achievable voltage ranges for both frequencies are compatible
193 at this point, as can be seen in Fig. 2(a).

194 For that m_a is 1, the normalized voltages (over V_{dc}) of $\hat{V}_{AB}^{f_C}$
195 and $\hat{V}_{AB}^{f_L}$ are drawn in Fig. 4 for changing $\Delta\theta_c$ and $\Delta\theta_r$. It is
196 observed that while the normalized voltages at f_C (f_2) can be
197 adjusted in the range of [0, 0.601], the normalized voltages at f_L
198 (f_1) can be adjusted in the range of [0, 0.318]. The normalized
199 voltage ranges are swapped if we use f_H instead of f_L . One of
200 these two operations can be selected or switched online based
201 on the required power ratings of the Rx sides.

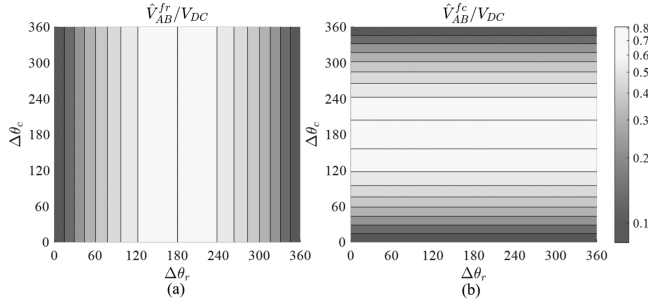


Fig. 5. Wideband operation. (a) Normalized voltage at f_R . (b) Normalized voltage at f_C .

202 D. Wideband Operation

203 In the wideband operation, the f_R component is used to
204 achieve the lower frequency (f_1), and f_C is used to obtain the
205 higher frequency component (f_2). The peak value of f_R and f_C
206 can be calculated in the phasor domain by using (2) and (4), and
207 they are given in (8) and (9)

$$\hat{V}_{AB^{fr}} = V_{dc} m_a \sqrt{\frac{1 - \cos(\Delta\theta_R)}{2}} \quad (8)$$

$$\hat{V}_{AB^{fc}} = V_{dc} \frac{2}{\pi} J_o \left(\frac{\pi}{2} m_a \right) \sqrt{1 - \cos(\Delta\theta_C)}. \quad (9)$$

208 In this operation, it is proper to select m_a as 0.8 since the
209 achievable voltage ranges for both frequencies are equal at
210 this point, as can be seen in Fig. 2(a). For that m_a is 0.8, the
211 normalized voltages (over V_{dc}) of $\hat{V}_{AB^{fr}}$ and $\hat{V}_{AB^{fc}}$ are drawn
212 in Fig. 5 for changing the control parameters of $\Delta\theta_C$ and $\Delta\theta_R$.
213 It is observed that both normalized voltages at f_R (f_1) and f_C
214 (f_2) can be adjusted in the range of [0, 0.81].

215 III. DISCUSSIONS AND FURTHER INVESTIGATIONS

216 A. Dual-Frequency Compensation System

217 A dual-frequency compensation system on the transmitter
218 side operates at both frequencies, while series capacitors set
219 the receiver sides to their respective resonant frequencies. This
220 article focuses specifically on dual-frequency excitation by using
221 the modulation method, so we present the values and the type of
222 compensation circuit employed rather than delving into the de-
223 sign of coil and compensation system, which can be found in the
224 literature [15], [16]. Fig. 1 shows the diagram of dual-frequency
225 compensation circuit, and Table II lists the circuit parameters of
226 both wideband and narrowband operations.

227 B. Gain Response and the Interference Between Receivers

228 The gain responses of receivers for narrowband and wideband
229 operations are shown in Fig. 6.

230 Notably, while almost no interaction occurs between the
231 receivers in a wideband operation, the narrowband operation
232 introduces mutual influence. This influence changes the effec-
233 tive gain for dual-frequency excitation, so the operating phase
234 shifts should be adjusted to account for this interference effect.
235 Moreover, optimization of the compensation method or proper

TABLE II
DUAL-RECEIVER WPT SYSTEM PARAMETERS

Parameters	Simulation value	Experimental value
Transmitter inductance	L_{TX}	$48\mu H$
Receiver inductances	L_{RX1}	$75\mu H$
Narrowband compensation inductance	L_{TX}	$1.5\mu H$
Wideband compensation inductance	L_{TX}	$28\mu H$
Narrowband transmitter compensation capacitances	C_{TX1}	$454pF$
Narrowband receiver compensation capacitances	C_{RX1}	$13.2nF$
Wideband transmitter compensation capacitances	C_{TX2}	$340pF$
Wideband receiver compensation capacitances	C_{RX2}	$236pF$
Narrowband load resistances	R_{L1}	68Ω
Wideband load resistances	R_{L2}	68Ω
Mutual inductance	M_1	$6\mu H$
	M_2	$6\mu H$

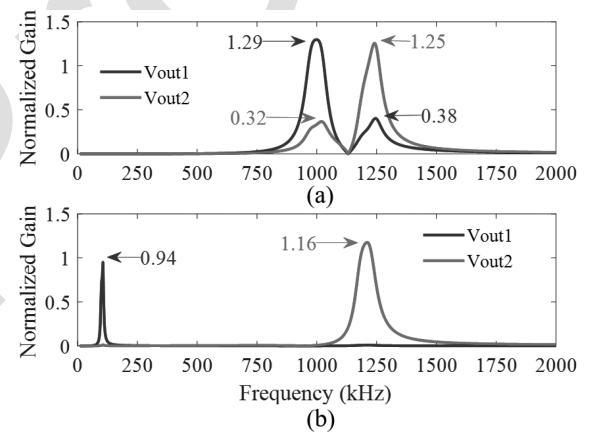


Fig. 6. Gain response of the dual receivers WPT system. (a) Narrowband operation. (b) Wideband operation.

TABLE III
DC-LINK UTILIZATION RATIO OF THE PROPOSED MODULATION TECHNIQUE

	Voltage gain at f_1	Voltage gain at f_2
Wideband operation	0.81	0.81
Narrowband operation	0.318	0.601

frequency selection can be recommended to mitigate this effect.
For example, anti-interference compensation on the receiver
sides might be suitable [17]. In addition, the cross-coupling
between receivers should be minimized, since it increases the
interference ratio.

241 C. DC-Link Utilization Ratio of the Proposed Modulation 242 Method

The proposed modulation allows for voltage control at two
243 frequencies, which are limited to specific dc-link utilization
244 ratio, which are given in Table III. The utilization ratios of the
245 dual frequency excitation vary based on frequency selection in
246 the other modulation techniques. In a system using superposition
247 in SPWM, the summation of two signals should be at a maximum
248 of 1 [13]. If you use antiphase signals, you can increase the
249 utilization ratio. In this article using SHEPWM, it is observed
250

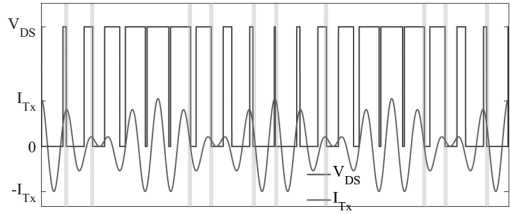


Fig. 7. Exemplary waveforms of drain-source voltage (V_{DS}) and transmitter current (I_{Tx}) with marked ZVS points in green. 10 of 20 turn-ON instances achieve ZVS.

that the utilization ratio typically range between 0.3 and 0.9 [8]. Moreover, when two distinct frequencies are excited with two half-bridges, a utilization ratio of $0.5 \times 4/\pi = 0.64$ can be achieved for both frequencies. Our recommended wideband modulation exceeds the gains of a two-half-bridge configuration. In the narrowband, one frequency could be excited with approximately these values while the other frequency component has a lower gain.

D. Dual-Receiver Output Regulation

The first control method in the proposed system is to adjust the carrier and reference phase shifts since you can change the voltage gain of the modulation. The second method is to detune the operating frequency since the proposed modulation technique can easily accommodate various frequencies. Furthermore, the active rectifiers at the receiver sides might be utilized to regulate the output voltages finely. In this article, the control loop is not closed, and the output voltages have been controlled by introducing phase shifts.

E. Zero Voltage Switching (ZVS) Conditions

Conventional WPT systems act as an inductive load, causing the current to lag when operating above the resonant frequency (unless in bifurcation condition). Before setting the gate signal high, a dead-time (blanking time) is given between each leg's top and bottom switches to prevent short-circuiting of the dc-link capacitors. During this dead-time period, the load current discharges the output capacitances of the switches. The inductive operation and lagged current ensure that the current direction always aligns with the discharging of the capacitors. As a result, the switches achieve ZVS at turn-ON. However, in the proposed system, the existence of multifrequency components in the transmitter current disrupts this assurance, even if the system operates in the inductive region at each frequency. Nevertheless, the proposed system may still have partial ZVS points, depending on the magnitudes and frequencies of the components of the Tx currents. An example operating point is depicted in Fig. 7, with the ZVS points marked.

Therefore, the system needs to be designed assuming hard-switching conditions. This design remains in the worst-case scenario. However, the efficiency might be higher in practical use than calculated, thanks to the partial ZVS.

F. Efficiency Analysis

The system's power losses are primarily due to the losses of inverter (P_{inv}), rectifier (P_{rec}), and network (P_{net}), as given in [18]. Then, overall system efficiency can be calculated by

$$\eta = \frac{P_{out}}{P_{in}} = \frac{P_{out}}{P_{out} + P_{inv} + P_{rec} + P_{net}} \quad (10)$$

where P_{in} is input power, and P_{out} is output power. First, the inverter loss can be split into two parts as given in

$$P_{inv} = P_c + P_{sw} \quad (11)$$

where P_c is the conduction loss, and P_{sw} is the switching loss. In conventional 1Tx–1Rx WPT systems, achieving ZVS, which reduces switching losses significantly, is ensured by operating in the inductive region near the zero-phase angle (ZPA). Then, the inverter loss, when in ZVS operation, can be considered conduction loss. However, in the proposed 1Tx–2Rx system, the ZVS might not be ensured, and the inverter loss should be calculated in hard-switching operation, as given by

$$P_{inv} = P_c = I_{Tx}^2 r_{ds} + f_{sw}(E_{sw-ZCS} + E_{sw-OL}) \quad (12)$$

where I_{Tx} is the rms value of the Tx current, r_{ds} is the MOSFET ON-state resistance, f_{sw} is the switching frequency, E_{sw-ZCS} is the zero current switching energy due to output capacitances of the switches, and E_{sw-OL} is the overlapping switching energy because of switching speed of switches as dv/dt and di/dt . Moreover, operating near ZPA can also decrease conduction losses by lowering the rms of the Tx current since the power factor becomes unity. Second, the rectifier operates in continuous conduction mode, resulting in pure sinusoidal current. Therefore, the loss can be calculated by

$$P_{rec} = \left(\frac{2\sqrt{2}}{\pi} V_F I_{Rx1} + r_F I_{Rx1}^2 \right) + \left(\frac{2\sqrt{2}}{\pi} V_F I_{Rx2} + r_F I_{Rx2}^2 \right) \quad (13)$$

where V_F and r_F are the opening voltage and ON-state resistance of the diodes, and I_{Rx1} and I_{Rx2} are receiver currents. Finally, the loss from network elements, such as passive elements, such as coils and capacitors, depends on the rms value and frequency of the currents of the Tx and Rx sides. The loss can be calculated by

$$P_{net} = I_{Tx}^2 r_{net_{Tx}} + I_{Rx1}^2 r_{net_{Rx1}} + I_{Rx2}^2 r_{net_{Rx2}} \quad (14)$$

where $r_{net_{Tx}}$, $r_{net_{Rx1}}$, and $r_{net_{Rx2}}$ are the representative resistances for network losses for the Tx and Rx sides.

The analysis conducted previously shows that the proposed system might have higher inverter loss than conventional 1Tx–1Rx systems due to the absence of ZVS. The other losses are almost equal to those of conventional systems if we make a fair comparison. Yet, the incorporation of wideband gap semiconductors plays a crucial role. It allows for an increase in the dv/dt , thereby reducing switching losses and enabling hard-switching opportunities at higher switching frequencies. Consequently, the overall system may have a switching loss that forms a minority portion of the total loss. In such a scenario, reducing costs

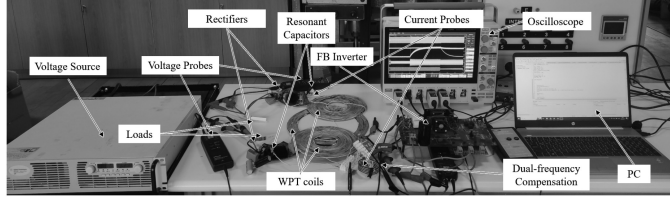


Fig. 8. Experimental setup of dual-mode WPT System.

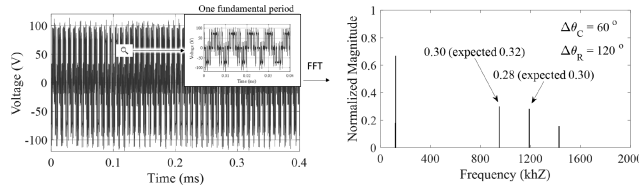


Fig. 9. Inverter output voltage and its harmonics spectrum for narrowband operation. The fundamental frequency is 119.5 kHz, and the switching frequency is 1190 kHz. The modulation index is 1.

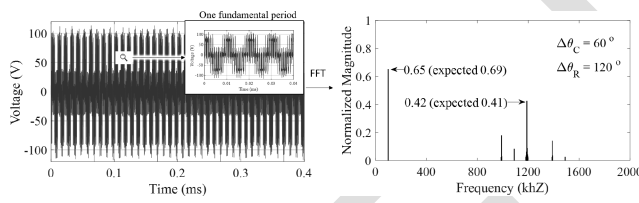


Fig. 10. Inverter output voltage and its harmonics spectrum for wideband operation. The fundamental frequency is 100 kHz, and the switching frequency is 1190 kHz. The modulation index is 0.8.

333 achieved by decreasing the number of inverters can offset the
334 efficiency decrease due to switching loss.

335 IV. EXPERIMENTAL VALIDATION

336 An experimental setup, shown in Fig. 8, is established to
337 validate the proposed system. The system parameters are shown
338 in Table II. In the setup, we wound the coils using 1 mm
339 diameter litz wires. The oscilloscope was a six-channel Tek-
340 tronix MSO46. We employed PEM CWTMini HF03B current
341 probes for ac current measurement and Tektronix THDP0100
342 differential probes for voltage measurement. The power sup-
343 ply was an Agilent N8739A. To generate the proposed mod-
344 ulation, the TI C2000 TMS320F28379D microcontroller is
345 utilized.

346 A. Dual-Mode Inverter Tests

347 The voltage waveforms of V_{AB} for both narrowband and
348 wideband operations are shown in Figs. 9 and 10. As expected, it
349 is observed that the voltages of each frequency can be indepen-
350 dently controlled by $\Delta\theta_R$ and $\Delta\theta_C$. There are slight differences
351 between experimental results and mathematical calculations,
352 which are at a maximum of 6%.

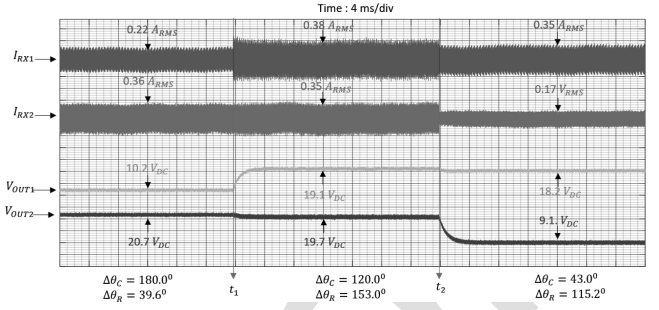


Fig. 11. Narrowband operation of dual-mode WPT system. m_a is 1, f_L is 951 kHz, and f_C is 1190 kHz.

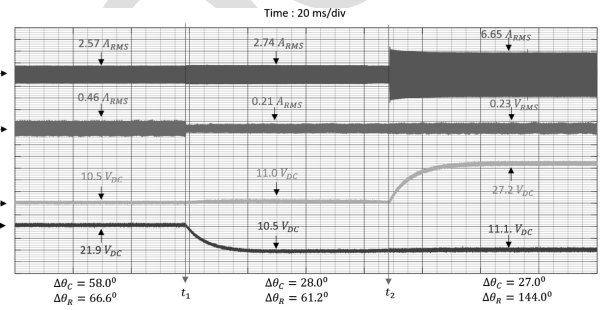


Fig. 12. Wideband operation of dual-mode WPT system. m_a is 0.8, f_R is 100 kHz, and f_C is 1190 kHz.

TABLE IV
POWER TRANSFER EFFICIENCIES FOR DIFFERENT OPERATING POINTS

	Carrier phase shift	Reference phase shift	Power transfer efficiency
Narrowband operation	180°	39.6°	74.6 %
	120°	153°	76.3 %
	43°	115.2°	76.0 %
Wideband operation	58°	66.2°	75.3%
	28°	61.2°	75.7 %
	27°	144.0°	75.5 %

B. Dual-Mode WPT System Tests

The Rxs and outputs' currents and V_{AB} voltage are obtained for narrowband and wideband operations, as given in Figs. 11 and 12. Transient analysis was performed to study the impact of different operating phase shifts in both wideband and narrowband operations. It's important to note that the voltages in this experimental setup may deviate slightly from the analytical calculations due to dead time and other nonlinearities since closed-loop control was not utilized. Furthermore, in narrowband operation, the interference between receivers necessitates minor updates to the phase shifts in addition to the analytical calculations in order to compensate for the effect.

C. Dual-Mode WPT System Power Transfer Efficiencies

The efficiency measurements for both narrowband and wideband operations in various conditions are provided in Table IV. In all cases, it was observed that the efficiencies were about 75%. Our proposed system has a key advantage that could potentially lead to increased efficiency by reducing the required switching

TABLE V
COMPARISON WITH EXISTING STUDIES IN THE LITERATURE

	Channel mode	Tx device	Offline algorithm	Operating frequency
[7]	2 (WB)	Two-2LC	NR	$= f_s$
[8]	2 (NB/WB)	Single-2LC	R	$\leq f_s$
[13]	2 (NB)	Single-2LC	NR	$< f_s$
[14]	2 (NB)	Single-MLI	NR	$\geq f_s$
This work	2 (NB/WB)	Single-2LC	NR	$= f_s$

2LC : Two level converter, MLI : Multi level inverter,

NB : Narrowband, WB :Wideband, R : Required, NR :Not required.

371 frequencies. Still, it is also worth considering optimizing the coil
372 and compensation systems to improve efficiency further.

373 V. COMPARISON WITH LITERATURE

374 Existing studies are compared with the proposed system in
375 Table V. Unlike the approaches presented in [7] and [14], our
376 proposed system does not require extra switches, which reduces
377 the cost and complexity. In contrast to the system discussed
378 in [13], our system allows both wideband and narrowband
379 operations and has operating frequencies near the switching
380 frequency, decreasing switching losses. Unlike the method out-
381 lined in [8], our system does not require an offline algorithm
382 to calculate the different quiescent points, thereby enabling
383 dynamic operations.

384 VI. CONCLUSION

385 In this letter, concurrent power transfer at dual frequency was
386 achieved by a single converter using a novel hybrid reference and
387 carrier phase shifts method of SPWM, allowing for a control-
388 lable dual-frequency output. This versatile modulation method
389 is applicable to narrowband and wideband operations, and it
390 enables the use of single Tx device by multiple standards. The
391 experimental setup was established to confirm the effectiveness
392 of the proposed modulation technique, and a good agreement
393 was observed between experimental results and mathematical
394 calculations. Further, the proposed system offers several advan-
395 tages, such as reduced switching components and lower switch-
396 ing frequency, resulting in increased efficiency and decreased
397 system cost. Consequently, the proposed system enhances the
398 adoption of dual-band WPT systems that support multistandard
399 usage in robotics and consumer electronics.

400 REFERENCES

- 401 [1] W. Jin, A. T. L. Lee, S.-C. Tan, and S. Y. R. Hui, "Single-inductor multiple-
402 output inverter with precise and independent output voltage regulation,"
403 *IEEE Trans. Power Electron.*, vol. 35, no. 10, pp. 11222–11234, Oct. 2020.

- [2] "The QI wireless power transfer system power class 0 specification," Apr. 2016. [Online] Available: <https://www.wirelesspowerconsortium.com/>
- [3] "Nxp wireless power solutions," NXP, May 2017. Accessed: Mar. 20, 2023. [Online]. Available: <https://www.nxp.com/docs/en/supporting-information/BL-Micro-NXP-Wireless-Charging-Solutions-Beta-Chen.pdf>
- [4] Y. Xiao, C. Liu, Y. Huang, and S. Liu, "Concurrent wireless power transfer to multiple receivers with additional resonant frequencies and reduced power switches," *IEEE Trans. Ind. Electron.*, vol. 67, no. 11, pp. 9292–9301, Nov. 2020.
- [5] J. Wu, L. Bie, W. Kong, P. Gao, and Y. Wang, "Multi-frequency multi-amplitude superposition modulation method with phase shift optimization for single inverter of wireless power transfer system," *IEEE Trans. Circuits Syst. I: Reg. Papers*, vol. 68, no. 5, pp. 2271–2279, May 2021.
- [6] *A Wireless Power Transfer System Baseline System Specification (BSS)*, Standard A4WP-S-0001 v1.3, Jan. 2014.
- [7] D. Ahn and P. P. Mercier, "Wireless power transfer with concurrent 200-kHz and 6.78-MHz operation in a single-transmitter device," *IEEE Trans. Power Electron.*, vol. 31, no. 7, pp. 5018–5029, Jul. 2016.
- [8] C. Zhao and D. Costinett, "GaN-based dual-mode wireless power transfer using multifrequency programmed pulse width modulation," *IEEE Trans. Ind. Electron.*, vol. 64, no. 11, pp. 9165–9176, Nov. 2017.
- [9] F. Liu, Y. Yang, Z. Ding, X. Chen, and R. M. Kennel, "A multifrequency superposition methodology to achieve high efficiency and targeted power distribution for a multiload MCR WPT System," *IEEE Trans. Power Electron.*, vol. 33, no. 10, pp. 9005–9016, Oct. 2018.
- [10] Z. Liu, M. Su, Q. Zhu, Y. Chao, S. Zang, and A. P. Hu, "A dual-frequency three-dimensional 3-D WPT system with directional power transfer capability at two separately regulated outputs," *IEEE Trans. Emerg. Sel. Topics Power Electron.*, vol. 11, no. 3, pp. 2514–2524, Jun. 2023.
- [11] C. Qi, S. Huang, X. Chen, and P. Wang, "Individual output voltage regulation method of multifrequency multireceiver simultaneous WPT systems with a single inverter," *IEEE Trans. Emerg. Sel. Topics Power Electron.*, vol. 11, no. 1, pp. 1245–1261, Feb. 2023.
- [12] W. Jin, A. T. L. Lee, S.-C. Tan, and S. Y. Hui, "A gallium nitride (GaN)-based single-inductor multiple-output (SIMO) inverter with multifrequency AC outputs," *IEEE Trans. Power Electron.*, vol. 34, no. 11, pp. 10856–10873, Nov. 2019.
- [13] C. Xia, N. Wei, H. Zhang, S. Zhao, Z. Li, and Z. Liao, "Multifrequency and multiload MCR-WPT system using hybrid modulation waves SPWM control method," *IEEE Trans. Power Electron.*, vol. 36, no. 11, pp. 12400–12412, Nov. 2021.
- [14] Y. Liu, C. Liu, X. Gao, and S. Liu, "Design and control of a decoupled multichannel wireless power transfer system based on multilevel inverters," *IEEE Trans. Power Electron.*, vol. 37, no. 8, pp. 10045–10060, Aug. 2022.
- [15] Z. Zhang, X. Li, H. Pang, H. Komurcugil, Z. Liang, and R. Kennel, "Multiple-frequency resonating compensation for multichannel transmission of wireless power transfer," *IEEE Trans. Power Electron.*, vol. 36, no. 5, pp. 5169–5180, May 2021.
- [16] C. Qi, H. Miao, Z. Lang, and X. Chen, "A generalized methodology to generate, amplify and compensate multi-frequency power for a single-inverter-based MF-MR-S-WPT system," *IEEE Access*, vol. 8, pp. 181513–181525, 2020.
- [17] X. Tian, J. Zhang, H. Wang, and S. M. Goetz, "Design and analysis of automatic modulation and demodulation strategy in wireless power and drive transfer system," *IEEE Trans. Ind. Electron.*, to be published, 2024, doi: 10.1109/TIE.2024.3406885.
- [18] H. Liu, L. He, and B. Cheng, "Powerless fractional-order tuning wireless power transfer system with zero phase angle input," *IEEE Trans. Circuits Syst. I: Reg. Papers*, to be published, 2024, doi: 10.1109/TCSI.2024.3404647.